Title
THE CONCEPT OF CAUSALITY IN IMAGE RECONSTRUCTION

Authors
Llacer, J.
Veklerov, E.
Nunez, J.

Publication Date
1988-09-01

Lawrence Berkeley Laboratory
UNIVERSITY OF CALIFORNIA

Engineering Division

Presented at the NATO Advanced Study Institute,
Povoa, Portugal, September 12–23, 1988

The Concept of Causality in Image Reconstruction

J. Llacer, E. Veklerov, and J. Nunez

September 1988

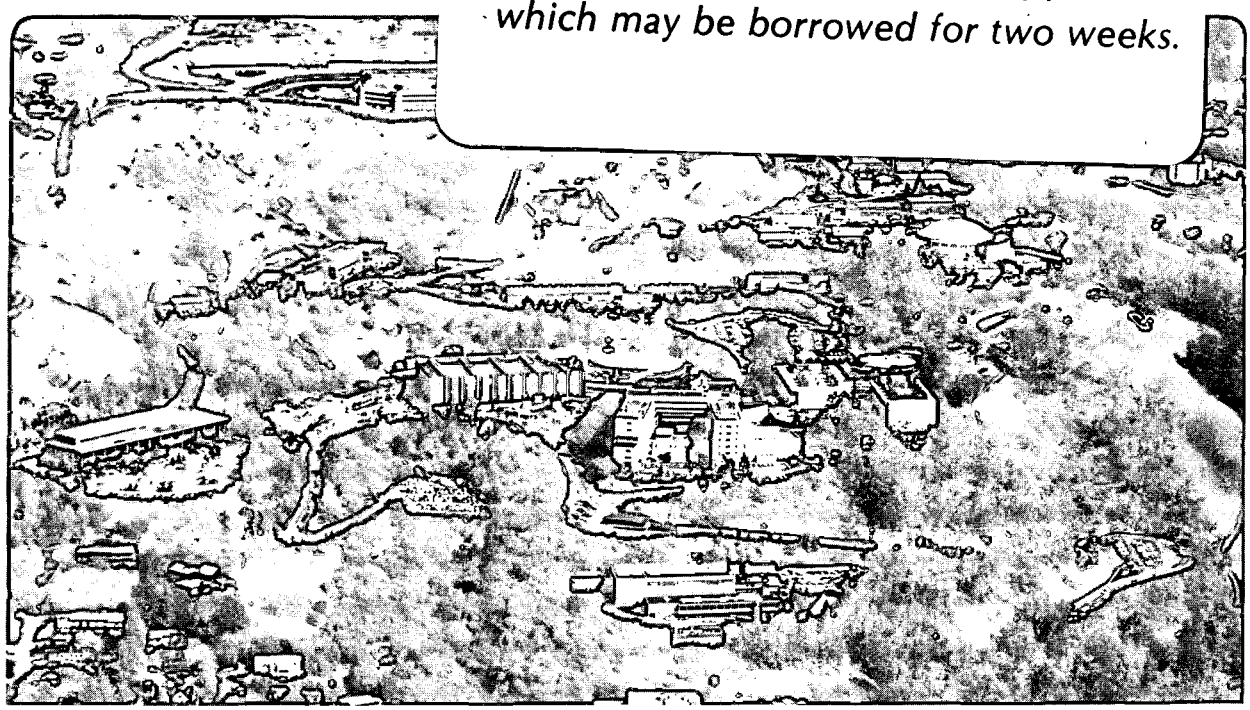

Prepared for the U.S. Department of Energy under Contract Number DE-AC03-76SF00098.

DISCLAIMER

THE CONCEPT OF CAUSALITY IN IMAGE RECONSTRUCTION

Jorge Llacer, Eugene Veklerov and Jorge Nunez[1]

Engineering Division
Lawrence Berkeley Laboratory
1 Cyclotron Road
Berkeley, CA 94720 USA

ABSTRACT

Causal images in emission tomography are defined as those which could have generated the data by the statistical process that governs the physics of the measurement. The concept of causality was previously applied to deciding when to stop the MLE iterative procedure in PET. The present paper further explores the concept, indicates the difficulty of carrying out a correct hypothesis testing for causality, discusses the assumption needed to justify the tests proposed and discusses a possible methodology for a justification of that assumption. The paper also describes several methods that we have found to generate causal images and it shows that the set of causal images is rather large. This set includes images judged to be superior to the best maximum likelihood images, but is also includes unacceptable and noisy images. The paper concludes by proposing to use causality as a constraint in optimization problems.

1. INTRODUCTION

Over the past two years we have been involved in a detailed study of the behavior of solutions to the image reconstruction problem in Emission Tomography (ET) by the Maximum Likelihood Estimator (MLE) and Maximum Entropy (ME) methods, with data generated both by computer simulation and by the ECAT-III tomograph of UCLA. Initially, the study focused on explaining the reasons for image deterioration after a certain number of iterations in the MLE method and on finding a cure for this problem.

As we progressed into the study of this phenomenon, we became aware of the fact that the observed deterioration is a direct consequence of trying to find an image which would have the highest probability of having generated

---

1) J. Nunez is on leave from the Faculty of Physics, University of Barcelona, Spain.

the initial noisy data (which the MLE is designed to do), but, in an apparent contradiction, a true radioactive source equal to the image found could not have yielded the experimental data by a Poisson disintegration process in a statistical sense. This contradiction results from the simple fact that the likelihood criterion favors images whose forward projections are as close to the data as possible, whereas the Poisson assumption imposes a certain deviation between the two.

Veklerov and Llacer (1987) observed that the images recovered after iterations within a certain range could have generated the data as ascertained by a hypothesis testing procedure that, upon further investigation, turns out to be based on an assumption discussed below. That initial finding led them to formulating a stopping rule for the MLE algorithm. We consider that for a radiologist to have confidence in the results of an image reconstruction, it is necessary but not sufficient that the recovered image, if it were a true emission source, could have generated the data. This has led Llacer and Veklerov (1988) to formulating the concept of causality. In this paper we explore that concept in some detail, discuss the difficulty in carrying out a correct test of causality within the framework of hypothesis testing, describe the assumption that must hold for the present tests to have statistical meaning and indicate a methodology that may justify that assumption. We are encouraged in that endeavor by the fact that causal images include some of the visually best reconstructions that we have seen, both from simulated and from true PET data.

2. DEFINITIONS OF CAUSALITY

In this section we define causality at three different levels of strictness without regard to the possible methods by which the hypothesis tests indicated or implied can be carried out. We also show schematically the region in projection space that includes causal images. Throughout this paper we shall use the standard notation introduced by Shepp and Vardi (1982):

$n^*(d),(d=1,\ldots,D)$	- the projection data or the number of coincidences detected in tube d;
$\lambda(b),(b=1,\ldots,B)$	- the emission density;
$p(b,d)$	- the transition matrix;
$\lambda^*(d) = \sum_{b=1}^{B} \lambda(b)p(b,d)$	- the means or forward projections;

where B and D are the number of pixels and the number of projections, respectively. We shall consider specifically the case of emission tomography (PET or SPECT) in which disintegration data follow Poisson statistics.

Definition 1: The image $\lambda(1), \lambda(2), \ldots, \lambda(B)$ is said to be a causal image with respect to data, $n^*(1), n^*(2), \ldots, n^*(D)$, if and only if the statistical hypothesis that $n^*(1), n^*(2), \ldots, n^*(D)$ is a Poisson sample with the means $\lambda^*(1), \lambda^*(2), \ldots, \lambda^*(D)$, respectively, can be accepted (not rejected).

The rationale behind Def. 1 is as follows: Let us assume that $\lambda^*(1) = \lambda^*(2) = \ldots = \lambda^*(D) = 100$ and all $n^*(d)$ are between 99 and 101. Then we have to conclude that the corresponding image is not causal because the deviation between the data and the means is less than what is imposed by the Poisson assumption. If, on the other hand, all $n^*(d)$ are either 50 or 150 in the same example, then the corresponding image is not causal either because the deviation between the data and the means is greater than what is imposed by the Poisson assumption. Put another way, a causal image is an image such that the distance between the data and the corresponding forward projection is "just right", not too small and not too large.

Definition 1 specifies the fullest form of causality or strong causality. That form appears difficult to implement as a constraint in an optimization problem. For that reason we introduce a new causality definition by relaxing Def. 1; since the new definition of causality requires less than Def. 1, it is appropriate to call this new form of causality "weak causality".

Definition 2: The image $\lambda(1), \lambda(2), \ldots, \lambda(B)$ is said to be a weakly causal image with respect to data, $n^*(1), n^*(2), \ldots, n^*(D)$, if and only if the second moments of $n^*(1), n^*(2), \ldots, n^*(D)$ are consistent with the Poisson hypothesis, namely:

$$\sum_{d=1}^{D} \frac{[n^*(d) - \lambda^*(d)]^2}{\lambda^*(d)} \simeq D \qquad (1)$$

Indeed, the expected value of the numerator of each term in Eq. (1) is the variance, while that of the denominator is the mean. Therefore, Eq. (1) must be satisfied if the Poisson hypothesis holds. However, the reverse statement is not true, because the equality of the variance and the mean is necessary but not sufficient for a distribution to be Poisson or, put another way, Def. 2 is less demanding than Def. 1.

It is possible to strengthen Def. 2 by requiring that higher moments of $n^*(1), n^*(2),\ldots, n^*(D)$ be consistent with the Poisson hypothesis as well.

Definition 3: The image $\lambda(1), \lambda(2),\ldots, \lambda(B)$ is said to be a k-causal image with respect to data, $n^*(1), n^*(2),\ldots, n^*(D)$, if and only if the first k moments of $n^*(1), n^*(2),\ldots, n^*(D)$ are consistent with the Poisson hypothesis, namely:

$$\sum_{d=1}^{D} \frac{[n^*(d) - \lambda^*(d)]^i}{f_i[\lambda^*(d)]} \simeq D \qquad (2)$$

where $i = 1,\ldots, k$ and $f_i(x)$ is the expression for the i-th moment of the Poisson distribution with the mean x.

The first moment meets this requirement automatically for any unbiased image. Here are the first several $f_i(x)$: $f_2(x) = x$, $f_3(x) = x$, $f_4(x) = 3x^2 + x$, $f_5(x) = 10x^2 + x$. Note that a 2-causal image is simply a weakly causal image and when $k \to \infty$, a k-causal image becomes strongly causal. The main advantage of Def. 3 over Def. 1 is that the former is easier to implement as a constraint of an optimization problem.

Geometrically, all weakly causal images belong to an area resembling an ellipsoid and surrounding the maximum likelihood point. Indeed, if the left-hand side of Eq. (1) must equal the right-hand side to the accuracy of ε, all points satisfying Eq. (1) form the space between two egg-shaped surfaces. We will call this space the causality shell. The k-causal and strongly causal images form a subset of the shell with gaps between them. Figure 1 shows an example of a shell as well as lines along which likelihood is constant, which are regular ellipsoids for large values of data.

3. THE TESTS FOR CAUSALITY

Let us outline the procedure for testing for strong causality described in detail by Veklerov and Llacer (1987). We will follow this outline with a critical discussion of its validity. We want to test the hypothesis that $n^*(1)$ is a realization drawn from a Poisson distribution with the mean $\lambda^*(1)$, $n^*(2)$ drawn from a Poisson distribution with the mean $\lambda^*(2)$, etc. A widely used method for testing such a hypothesis, known as Pearson's goodness of fit tests, see e.g. Canavos (1984), is to define several mutually

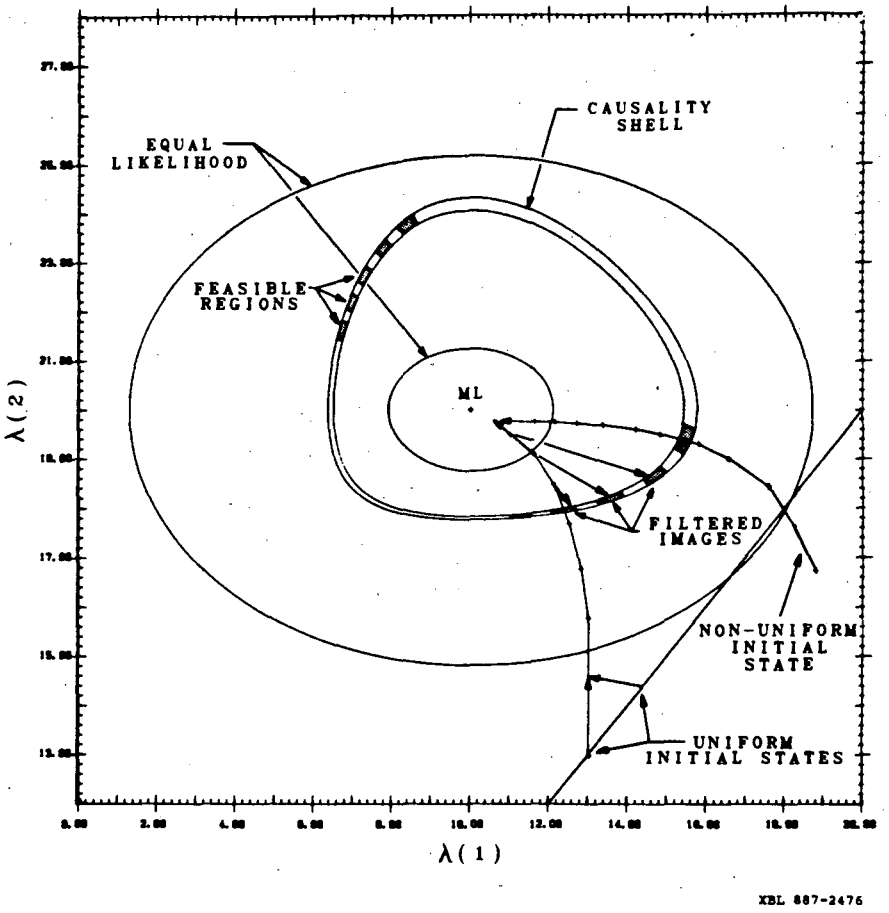

Fig. 1: Causality shell and ellipses along which likelihood is constant. MLE paths for different initial images. The results of filtering of "overdone" images after different MLE iterations are found to be causal.

exclusive and exhaustive classes, assign each realization to a class and then compare the observed numbers of realizations assigned to the classes with the expected numbers determined by the Poisson hypotheses. The discrepancy between the two is measured by the chi-square statistic. When the chi-square statistic exceeds a certain threshold, the hypothesis is rejected. Some technical difficulties arise in trying to adapt Pearson's procedures to our needs, but they are resolved in our previously referenced work.

A fundamental objection to the above procedure (pointed out to us by several workers) stems from the fact that the image which we are trying to test against has been generated by the same set of data that we are testing. Under those conditions, the question implied by testing for any of the definitions of causality given above cannot even be posed. Cramer (1946) proves that the chi square test, when certain parameters that describe

the function against which we are testing are estimated from the sample, can only be used to test the hypothesis that the data are drawn from the defined probability distribution with some values of those parameters. In our case this implies that, with the parameters $\lambda^*(d)$ having been derived from the data $n^*(d)$, we can only test the hypothesis that the data were obtained from a Poisson distribution with some values of $\lambda^*(d)$ unknown to us.

This limited test seems totally unnecessary since we know that the data were really generated by a Poisson disintegration process. It follows that, by using the appropriate number of degrees of freedom, a hypothesis test comparing the parameters $\lambda^*(d)$ generated by the MLE method (at convergence) to the data $n^*(d)$ should never be rejected if, indeed, the MLE is a good method for estimating those parameters. We shall pursue this test in the future.

The hypothesis tests that can be derived from the above definitions of causality would have complete validity if the parameters that determine the Poisson process against which we are testing were completely and independently specified. In our case that implies that we have a complete and independent knowledge of the activity distribution that generated the data. If that were the case, a test would again be unnecessary. We know that the data would have been generated by such a source distribution. Indeed, the whole image reconstruction process would be unnecessary.

Because of our observations that images generated by the MLE (and other methods as described below), when started from a uniform image field and stopped according to the rule derived from strong causality hypothesis testing, are visually good, with a useful compromise between edge sharpness and low noise in regions of high activity, we have to believe that our concept of causality, although not fitting correctly in the framework of hypothesis testing, has a definite value. Results similar to ours have also been obtained by Hebert et al (1988) in Single Photon Emission Tomography (SPECT). Many other researchers (mostly in the field of Astronomy) have come up with variations of the same tests which they proposed to use as constraints or necessary conditions for image reconstruction, or as an analysis of residues: Skilling and Bryan (1984), Ables (1974), Gull and Daniel (1978), Narayan and Nityanda (1986), Reiter and Pfleiderer (1986) and Tarantola (1987).

The assumption that we believe can lead to a justification of our hypothesis testing is related to the case of a completely specified image, as indicated above, and is the following:

> We are given an image and its projection $\lambda^*(d)$. We do not know how it was obtained. We are also given a set of data $n^*(d)$ and we are asked to test the hypothesis that that image, as if completely specified, could have generated the data. We would then proceed with testing the hypothesis in the methods developed or implied for Definitions 1 through 3.

The above assumption would be justified in practice if an analysis of the distribution of the hypothesis testing function H of Veklerov and Llacer (1987) (for Def. 1) or of the chi square function values (for Def. 2) for reconstructions of a large number of different realizations of a fixed image source distribution were found to be chi square distributed with the expected number of degress of freedom. Such a finding would imply that the strict theory of hypothesis testing can be relaxed under some conditions. We are now beginning such a study.

4. ARE ALL CAUSAL IMAGES GOOD?

The causal images obtained by stopping the MLE algorithm at the right point by no means exhaust the set of causal images. We have conducted two series of experiments in order to get an idea of how different causal images can be from one another. We have used a mathematical brain-like phantom with 1 million counts shown in Fig. 5a.

The first series consisted of images generated by the same MLE algorithm but with drastically different initial images. We chose a four quadrant checkerboard image as an initial image with 1.95 and 0.05 times the average number of counts per pixel in the "hot" and "cool" quadrants, respectively.

It converged towards the same maximum likelihood image as in the case of a uniform initial image, but its MLE path crossed the shell at a different point, as is shown schematically in Fig. 1. Visually, a causal image obtained with the checkerboard image used as the initial one still retains the boundaries between the quadrants. Figure 2a shows the image after iteration 2, and 2b shows it after iteration 50, where the image is causal (H = 15.2). The quadrant boundaries gradually disappear as the iterative process progresses but they are still visible at iteration 300.

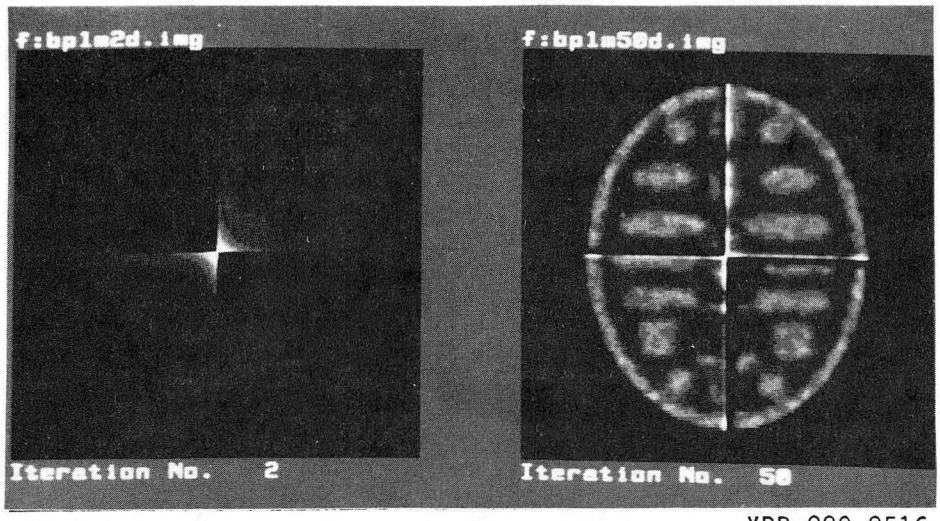

XBB 889-8516

Fig. 2: MLE reconstructions with the initial image being a 4 quadrant checkerboard. Image a) is after iteration 2; Image b) is after iteration 50; it is causal (H = 15.2).

The second series of experiments owes its origin to the idea put forth in Snyder et al (1987), whereby the use of a sieve and a resolution kernel is equivalent to post-filtering of the image generated by the regular MLE algorithm. Using that idea, we were able to produce a number of causal images as follows. We let the MLE process overshoot the causality shell. Thereafter, several "overdone" images were filtered by convolution with Gaussian distributions. By choosing the right standard deviations of the Gaussian distributions we were able to bring the images back to the shell, as is also shown schematically in Fig. 1.

It is interesting to note that it was necessary to use different values for the standard deviation to bring different MLE images back to the shell: the greater values were needed for images generated after more iterations. Figure 3 shows the value of the H function as a function of the standard deviation σ for several MLE images used in the convolution operation. The resulting causal images are shown in Fig. 4. Causal images obtained by filtering reconstructions with an increasing number of iterations show increasing noise. Image a) is a causal MLE image obtained by the stopping rule, image b) is an "overdone" MLE image after 50 iterations, images c), d), e) and f) are MLE images after 50, 100, 200 and 300 iterations, respectively, filtered to make them causal. The cleanest and sharpest image is image c). Furthermore, it is the "best" image we have ever seen for the data set at hand.

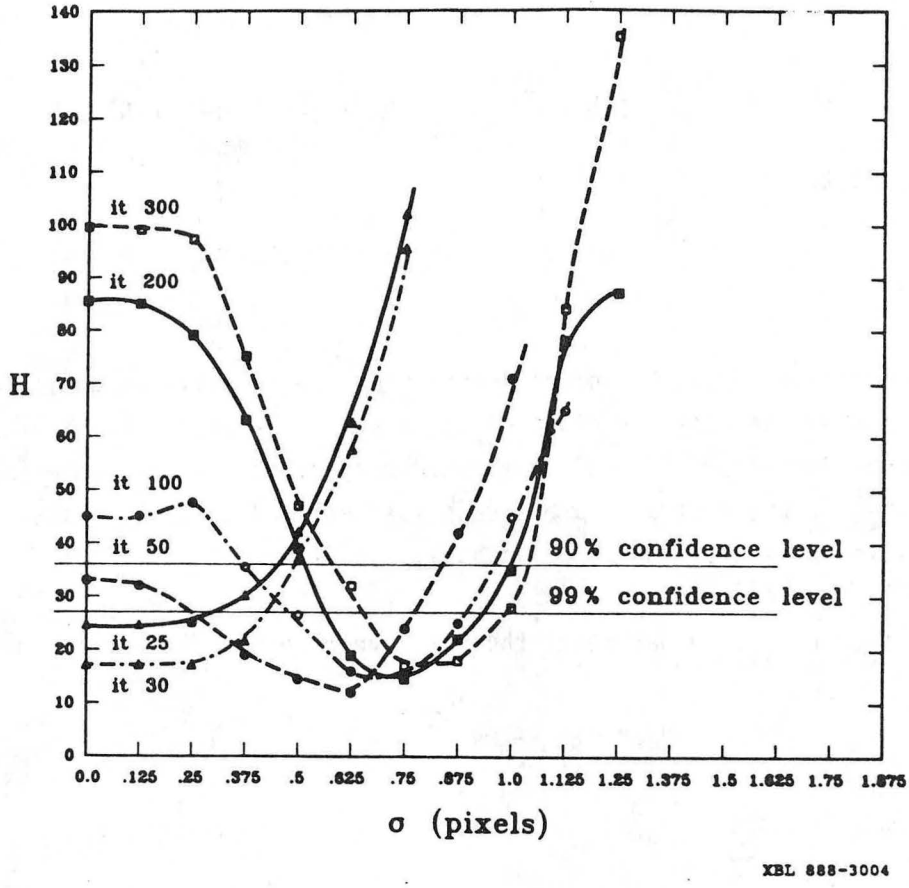

Fig. 3: Results of Gaussian filters with different standard deviations applied to MLE reconstructions after certain iteration numbers: 25, 30, 50, 100, 200 and 300. The hypothesis testing parameter H of the resulting images is shown as a function of the standard deviation. Different curves correspond to different iteration numbers.

5. MAXIMUM ENTROPY RECONSTRUCTION AND CAUSALITY

Another attempt to arrive at causal images was made by the use of maximum entropy techniques. The maximum entropy solution seems attractive because it yields the image with the lowest information content compatible with the data. Thus, the criterion will give an image which avoids any bias while satisfying the imposed constraints.

Following Frieden (1972) and Gullberg and Tsui (1987), we formulate the problem as follows:

Maximize:

$$-\sum_{b=1}^{B} \frac{\lambda(b)}{N_\lambda} \ln \frac{\lambda(b)}{N_\lambda} - \rho \sum_{d=1}^{D} \frac{n(d)}{N_n} \ln \frac{n(d)}{N_n} \qquad (3)$$

where

$$N_\lambda = \sum_{b=1}^{B} \lambda(b); \quad N_n = \sum_{d=1}^{D} n(d); \; \lambda(b) \geq 0; \; n(d) \geq 0$$

subject to

$$\sum_{b=1}^{B} P(b,d)\lambda(b) + n(d) - n_m = n^*(d); \; d=1,\ldots, D \qquad (4)$$

The parameter ρ is the weight quantifying the relative importance of the entropy of the noise vs. that of the image. The true noise or the difference between the data and the forward projections can be represented as $n(d) - n_m$, where $n(d)$ is a biased noise term and n_m is a constant noise bias which insures that $n(d)$ is always positive.

Due to the Poisson nature of the data, we have chosen:

$$n_m = \max \left[2\sqrt{n^*(d)}\right] \; d = 1,\ldots, D$$

and

$$\frac{\sum_{d=1}^{D} (n(d) - n_m)}{D} = 0 ; \qquad N_n = \sum_{d=1}^{D} n(d) = D\, n_m$$

The constant ρ effectively controls the smoothness of the solution: the larger the constant, the less smooth image will result for a given noise. If the data contains very little noise, ρ can be made very high thus obtaining high sharpness. The bias n_m also controls the smoothness of the image. In this case, the large n_m, the smoother the image, with a background being higher.

Note that in this model, the noise $n(d)$ is a variable in the optimization problem and the solution gives unbiased estimates for both the image and the noise. However, the present model does not contain the information about the Poisson nature of the data.

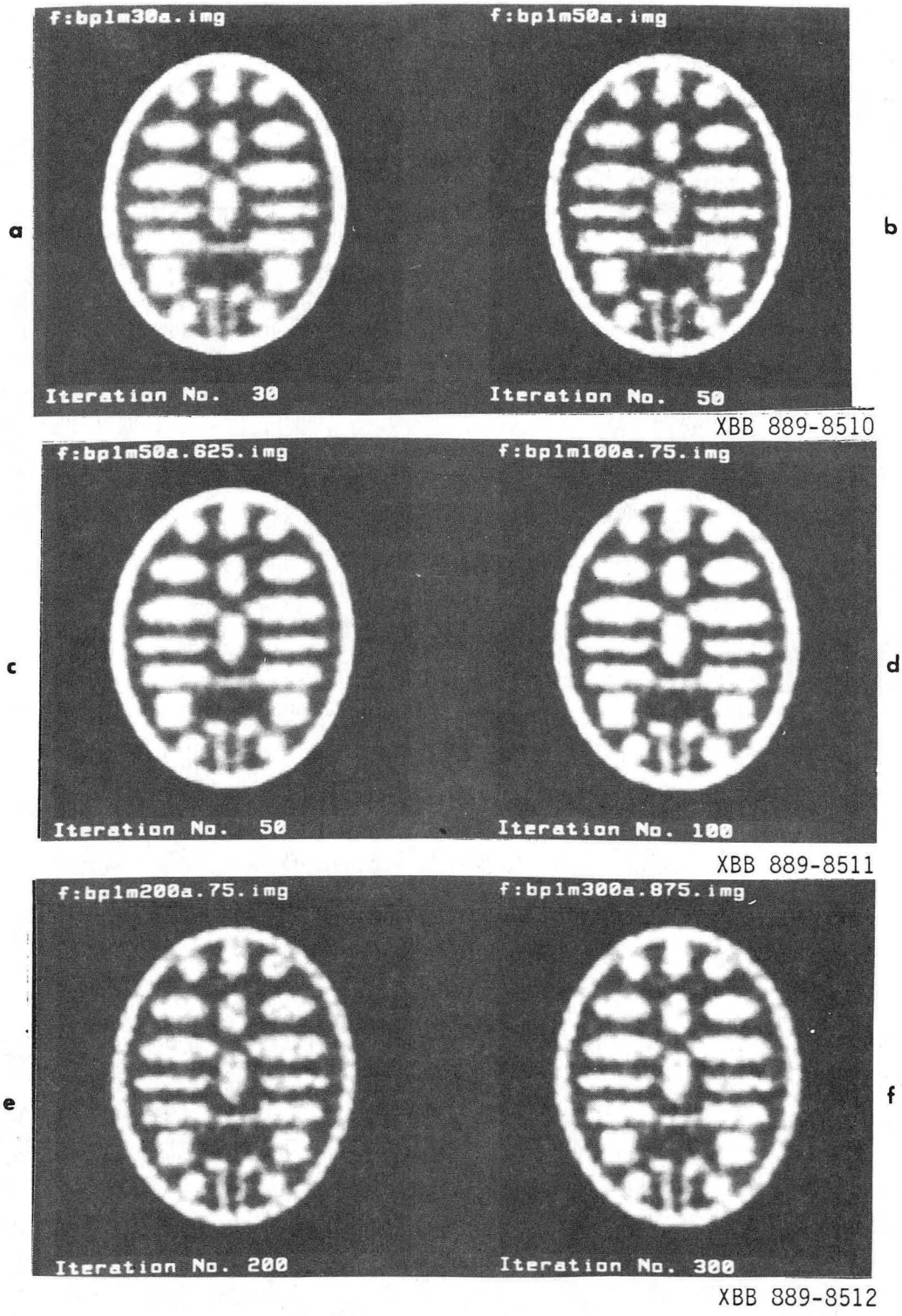

Fig. 4: Causal images obtained by the MLE or the MLE and subsequent filtering. a) MLE and the stopping rule (30 iterations, H = 17.5); b) MLE in the rising part of H (50 iterations, H = 30.25); c) is image b) filtered with sigma = 0.625 with resulting H = 13.2; d) MLE image after 100 iterations filtered with sigma = 0.75; e) MLE image after 200 iterations filtered with sigma = 0.75; f) MLE image after 300 iterations filtered with sigma = 0.875. Images d), e) and f) are all causal but with increasing noise.

In order to solve the problem of maximizing Eq. (3) subject to constraints in Eq. (4), we introduce the Lagrangian function and solve the unconstrained problem of maximizing:

$$L = -\sum_{b=1}^{B} \frac{\lambda(b)}{N_\lambda} \ln \frac{\lambda(b)}{N_\lambda} - \rho \sum_{d=1}^{D} \frac{n(d)}{N_n} \ln \frac{n(d)}{N_n}$$

$$- \sum_{d=1}^{D} \mu_d \left[n^*(d) - n(d) + n_m - \sum_{b=1}^{B} P(b,d)\lambda(b)\right] \frac{1}{N_\lambda}$$

where $\mu(d)$ $d = 1, \ldots, D$ are Lagrange multipliers.

The maximum of L is achieved when:

$$\frac{\partial L}{\partial \lambda(b)} = 0 \qquad b = 1, \ldots, B$$

$$\frac{\partial L}{\partial n(d)} = 0 \qquad d = 1, \ldots, D$$

$$\frac{\partial L}{\partial \mu(d)} = 0 \qquad d = 1, \ldots, D$$

which have the following solution:

$$\lambda(b) = N_\lambda e^{-1} \prod_{d=1}^{D} e^{P(b,d)\mu(d)}$$

$$n(d) = N_n e^{-1} e^{\mu(d) N_\lambda / \rho N_n} \tag{5}$$

where the Lagrange multiplier is determined by the system of D nonlinear equations:

$$N_\lambda e^{-1} \sum_{b=1}^{B} P(b,d) \prod_{m=1}^{D} e^{P(b,m)\mu(m)}$$

$$+ N_n e^{-1} e^{\mu(d) N_\lambda / \rho N_n} - n_m - n^*(d) = 0 \qquad d = 1, \ldots, D \tag{6}$$

The solution of the system as shown in Eq. (6), is derived using the nonlinear Gauss-Seidel-Newton iterative algorithm found in Ortega and Rheinboldt (1970). As the iterative algorithm for obtaining the Lagrange multipliers progresses, we can substitute the multipliers in Eq. (5) and monitor the formation of the image as well as its various statistics.

Figure 5b shows the maximum entropy reconstruction of the same phantom as the one used in the previous reconstructions in the absence of noise at convergence after 10 iterations with $\rho = 50$. Note that the reconstruction is nearly perfect. This shows that the algorithm works very well in the case of little noise where it is possible to use large values of ρ thereby achieving high sharpness in the reconstructed image.

In the presence of noise, the behavior of the present version of the algorithm is not adequate due to the simplicity of the noise model. We have obtained promising results by adjusting ρ and smoothing the final image.

The images in Figure 5c through 5f are the ME reconstructions of the same phantom of 5a with noise (Poisson data), with $\rho = 8$. Image c) is generated after only one iteration in the calculation of the Lagrange multiplier and d) after twenty iterations at convergence. Image e) is obtained by filtering image d) by convolving it with the Gaussian distribution with $\sigma = 0.75$ pixels. Image f) is obtained by increasing the bias parameter n_m by 25% and filtering. Note that the structures of the phantom are clearly visible but we have found that none of the images are causal.

We have just recently concluded the first reconstruction experiments with a fully Bayesian reconstruction method, using an entropy prior distribution and the Likelihood criterion as the conditional probability of the data, given an image. An adjustable parameter which, in effect, changes the weight of one of the criteria with respect to the other and appears justifiable in terms of intensity jumps of the image and data has been used in the problem formulation. This work is still in progress but we can report that, by proper choice of the adjustable parameter, it is possible to obtain images that converge (in an iterative formulation of the reconstruction process) to stable causal images of a quality very similar to that of the MLE images of Fig. 4 c). We have, thus, another method to obtain causal images.

6. CAUSALITY-BASED ALGORITHMS

The experiments described in Sect. 4 have demonstrated that the set of causal images is rather large. It includes the best images we have ever seen, which are clearly superior to MLE images, but it also includes unacceptable images as well as noisy ones. This suggests that causality is a valuable concept in image reconstruction but, taken alone, it is not enough to guarantee good reconstructions.

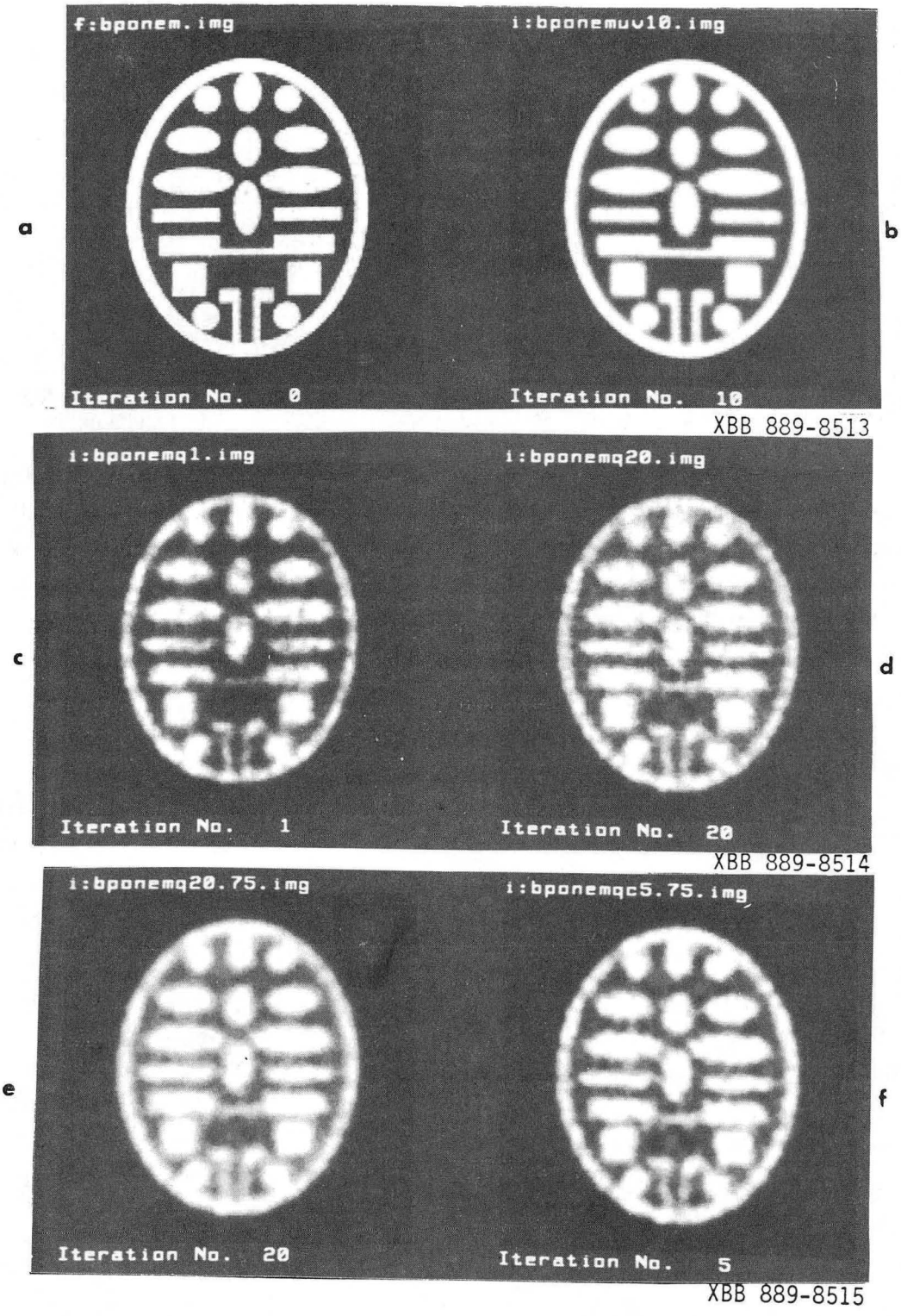

Fig. 5: ME images. a) source image with 1M counts; b) reconstruction with noiseless data; c) 1st iteration for obtaining Lagrange multipliers with H = 103; d) 20th iteration in Lagrange multipliers with very high H; e) 20 iterations filtered with sigma = 0.75 with H still too high (1142); f) obtained by increasing the bias parameter by 25% and filtering.

Therefore, it is promising to use causality as a constraint and try to optimize another criterion, such as entropy, while remaining on the shell. Then it may be more convenient, from the computation complexity point of view, to limit ourselves to weak or k-causality, that is:

Maximize:

$$-\sum_{b=1}^{B} \lambda(b) \ln \lambda(b)$$

subject to

$$\sum_{d=1}^{D} \frac{[n^*(d) - \lambda^*(d)]^i}{f_i[\lambda^*(d)]} \simeq D$$

for $i = 1, \ldots, k$.

This approach has been proposed by Skilling and Bryan (1984) who, using our terminology, considered only weak causality ($k = 2$) and in the Gaussian rather than Poisson case.

ACKNOWLEDGMENTS

This work has benefited from discussions which J. Llacer has held with J. Skilling, S. Gull, D. Snyder and M. Miller. The authors are particularly grateful to Harrison Barrett for persistent and fair criticism of the work leading to the present paper, resulting in a much better understanding of the essential nature of the problem.

This work has been supported by a grant from the National Cancer Institute (CA-39501) and the U.S. Department of Energy under Contract No. DE-AC03-76SF00098. The work of J. Nunez has been supported in part by the Catalan Studies Program (U. of California and the Generalitat de Catalunya).

REFERENCES

Ables. J.G., (1974). Maximum entropy spectral analysis, Astron. Astrophys. Suppl., 15, pp. 383-393.

Cavanos, G., (1984). Applied probability and statistical methods, Little, Brown & Co.

Cramer, H., (1946). Mathematical Methods of Statistics, Princeton University Press.

Frieden, B.R., (1972). Restoring with maximum likelihood and maximum entropy, J. Opt. Soc. Am., 62, pp. 511-518.

Gull, S.F. and Daniell, G.J.,(1978). Image reconstruction from incomplete and noisy data, Nature, 272, pp. 686-690.

Gullberg, G.T. and Tsui, B.M.W., (1987). Maximum entropy reconstruction with constraints: iterative algorithms for solving the primal and dual programs, Proc. of Xth International Conference on Information Processing in Medical Imaging, Ultrecht, The Netherlands, pp. 181-199.

Hebert, T., Leahy, R. and Singh, M., (1988). Fast MLE for SPECT using an intermediate polar representation and a stopping criterion, IEEE Trans. Nucl. Sci., Feb. 1988.

Llacer, J. and Veklerov, E., (1988). The use of a stopping rule in iterative image reconstruction, LBL Report LBL-25314, presented at the 1988 AMS-IMS-SIAM Conference on Spatial Statistics and Imaging, to be publ.

Narayan, R. and Nityananda, R., (1986). Maximum entropy image restoration in astronomy, Ann. Astron. Astrophys., 24, pp. 127-170.

Ortega, J.M. and Rheinboldt, W.C., (1970). Iterative solutions of nonlinear equations in several variables, Academic Press, New York.

Reiter, J. and Pfleiderer, J., (1986). Improvement of MEM-deconvolution by an additional constraint, Astron. Astrophys., 166, pp. 381-392.

Shepp, L.A. and Vardi, Y., (1982). Maximum likelihood reconstruction for emission tomography, IEEE Trans. Med. Imaging, MI-1, pp. 113-122.

Skilling, J. and Bryan, R.K., (1984). Maximum entropy image reconstruction: general algorithm, Mon. Not. R. Astr. Soc, 211, pp. 111-124.

Snyder, D.L., Miller, M.I., Thomas, L.J. and Pollite, D.G., (1987). Noise and edge artifacts in maximum-likelihood reconstructions for emission tomography, IEEE Trans. Med Imaging, MI-6, pp. 228-238.

Tarantola, A., (1987). Inverse problem theory, Elsevier.

Veklerov, E. and Llacer, J., (1987)., Stopping rule for the MLE algorithm based on statistical hypothesis testing, IEEE Trans. Med. Imaging, MI-6, pp. 313-319.

LAWRENCE BERKELEY LABORATORY
TECHNICAL INFORMATION DEPARTMENT
UNIVERSITY OF CALIFORNIA
BERKELEY, CALIFORNIA 94720